

## Analytical Dynamic Modelling of Heel-off and Toe-off Motions for a 2D Humanoid Robot

Majid Sadedel, Aghil Yousefi-koma\* and Faezeh Iranmanesh

*Center of Advanced Systems and Technologies (CAST), School of Mechanical Engineering, College of Engineering,  
University of Tehran, Tehran, Iran.*

Received 13 September 2015; Accepted 11 November 2015

### Abstract

The main objective of this article is to optimize the walking pattern of a 2D humanoid robot with heel-off and toe-off motions in order to minimize the energy consumption and maximize the stability margin. To this end, at first, a gait planning method is introduced based on the ankle and hip joint position trajectories. Then, using these trajectories and the inverse kinematics, the position trajectories of the knee joint and all joint angles are determined. Afterwards, the dynamic model of the 2D humanoid robot is derived using Lagrange and Kane methods. The dynamic model equations are obtained for different phases of motion and the unknowns, including ground reactions, and joint torques are also calculated. Next, the derived dynamic model is verified by comparing the position of the ZMP point based on the robot kinematics and the ground reactions. Then, the obtained trajectories have been optimized to determine the optimal heel-off and toe-off angles using a genetic algorithm (GA) by two different objective functions: minimum energy consumption and maximum stability margin. After optimization, a parametric analysis has been adopted to inspect the effects of heel-off and toe-off motions on the selected objective functions. Finally, it is concluded that to have more stable walking in high velocities, small angles of heel-off and toe-off motions are needed. Consequently, in low velocities, walking patterns with large angles of heel-off and toe-off motions are more stable. On the contrary, large heel-off and toe-off motions lead to less energy consumption in high velocities, while small heel-off and toe-off motions are suitable for low velocities. Another important point is that for the maximum stability optimization, compared to minimum energy consumption optimization, more heel-off and toe-off motions are needed.

**Keywords:** *dynamic model, gait optimization, heel-off and toe-off motions, humanoid robot.*

### 1. Introduction

In robotic studies, one of the most challenging problems, which is the main goal of the design and fabricating a humanoid robot, is achieving a fast, human-like, and stable walking in

different environments. To this end, some preliminary steps are needed. Normally, the first step is the gait planning. Developing a walking pattern, in spite of all constraints and necessities, gives us a wide variety of choices. To choose the best and the optimum gait

---

\* Corresponding Author E-mail: aykoma@ut.ac.ir

among all choices, some criteria are needed. Some of them are dynamic-based performance criteria, e.g., joint actuating torques [1] and energy consumption [2].

There are two major methods for walking gait planning of a humanoid robot: online and offline. In online path planning, all computations are done during the robot motion. This will increase calculation costs, which is an important problem. Necessarily, some simplified models of robots, such as inverted pendulum model [3], cart table model [4], two masses model [5] and three masses model [6] are used.

In offline path planning, all walking patterns, which have been calculated in advance, are stored in a memory card. Since walking pattern generation is an offline process, a full dynamic model could be used, which is one of the most advantages of this method [7]. It should be noted that both online and offline methods need an online control algorithm to reject the disturbance while walking.

Almost all the optimization criteria, such as energy consumption, maximum torque, maximum power, speed, stability, etc. are directly or indirectly related to the robot dynamic model [2, 8-12]. On the other hand, using an appropriate and accurate dynamic model leads to an improved hardware selection. An identical utilization could be seen in Carbone and Buschmann studies [13, 14].

The dynamic model may be obtained by different methods. Some of the recent studies are based on Lagrange or Kane methods [15-21]. Others have used Newton-Euler approach, demanding lower computational load, but calculate all components of joint reacting forces and moments, which is not needed here [13, 22-24].

To analyze the stability of a humanoid robot, different criteria are suggested. ZMP<sup>1</sup> is the mostly used stability criterion in humanoid robot which will be employed in this paper. This criterion was first introduced by Vukobratovicin in 1969 [25]. Other stability criteria are FRI [26], MFRI [27], and CWC [28].

In this paper, first an offline path planning algorithm is introduced to calculate the trajectories of joint angles. Then, the robot dynamic equations are derived using two

analytical approaches: Kane and Lagrange methods. These two approaches are used to develop a dynamic model for different walking phases. Finally, two verifications are done; First, by comparing the Kane and Lagrange methods' results and, then, by adopting a stability criterion. In other words, the position of ZMP point is calculated by two different methods and the results are compared to verify the dynamic model. In the last section, the optimization process is done using GA. Some parameters are selected as the optimization parameters and two different objective functions are used to be optimized. At the end, the results of these two optimizations are compared.

## 2. Model Features and Gait Planning

In this section, the procedure of gait planning of a 2D humanoid robot is described. The modelled Robot is a 2D humanoid Robot with 7 links and 6 DOFs. Each leg has 3 DOFs. Each hip, knee, and ankle joints have 1 DOF. The schematic of this 2D humanoid robot has been shown in Figure 1.

The parameters of the studied model, representing the characteristics of the robot, are shown in Table 1 and Table 2. It should be noted that the moment of inertia of each link is calculated with respect to its center of mass. The values of these parameters are according to SURENA III, a humanoid robot designed and fabricated at the Center of Advanced Systems and Technologies (CAST), located at the University of Tehran.

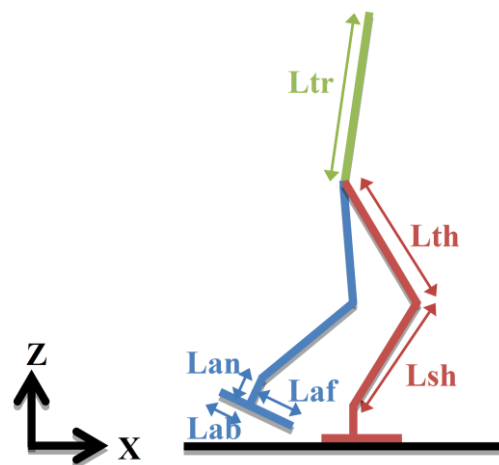


Fig. 1. Schematic of a biped robot with 7 links and 6 DOFs

1. Zero Moment Point

Table 1. Length of the links

Parameter	Length (m)
$L_{tr}$	0.630
$L_{th}$	0.360
$L_{sh}$	0.360
$L_{an}$	0.093
$L_{af}$	0.099
$L_{ab}$	0.163

Table 2. Mass and moment of inertia of the links

Link	Mass(Kg)	Moment of Inertia (Kg.m <sup>2</sup> )
Trunk	20.15	0.251
Thigh	4.43	0.054
Shank	3.49	0.063
Foot	3.25	0.029

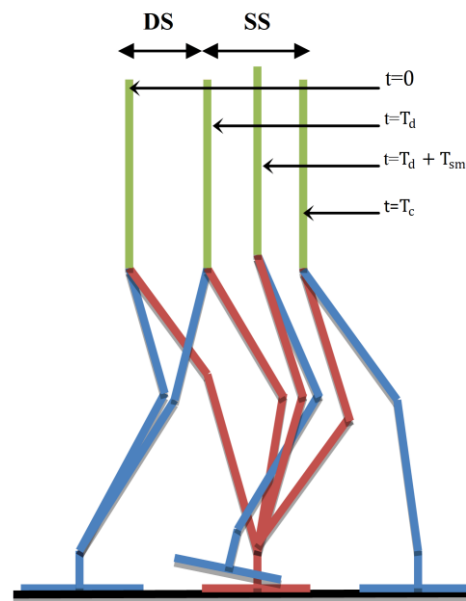


Fig. 2. Walking phases

Table 3. Walking pattern parameters

Parameters	Values	Dimension	Description
$T_d$	$0.4T_c$	Second	DSP time period
$T_s$	$T_c - T_d$	Second	SSP time period
$T_{sm}$	$0.4T_s$	Second	Middle time in SSP
$T_{dm1}$	$0.3T_d$	Second	First middle time in DSP
$T_{dm2}$	$0.7T_d$	Second	Second middle time in DSP
$T_c$	$D_c/V$	Second	Walking step period
$q_{ff}$	10	Degree	Orientation of heel at the start of DSP (heel-off angle)
$q_{fm}$	0	Degree	Orientation of swing foot with respect to ground at $T_{sm}$
$q_{fb}$	10	Degree	Orientation of toe at the end of DSP (toe-off angle)
$x_{ed}$	$0.15D_c$	Meter	Distance between hip and support ankle at the end of SSP
$x_{sd}$	$0.1D_c$	Meter	Distance between hip and support ankle at the start of SSP
$Z_{h-min}$	$0.87(L_{an} + L_{sh} + L_{th})$	Meter	Minimum hip height
$Z_{h-max}$	$0.9(L_{an} + L_{sh} + L_{th})$	Meter	Maximum hip height
$D_c$	0.4	Meter	Step length

The motion of the robot is consisted of two phases: single support (SS) and double support (DS), which are illustrated in Figure 2. Different walking pattern parameters are introduced in Table 3.

In this section, path planning for the gait with heel-off and toe-off motions is presented. The first step is to generate the position trajectory of ankle and hip joints. Some notable

hints should be considered in this step. As the robot moves, the feet will not penetrate the level ground; also the generated spline curves should satisfy the continuity of speed and acceleration. Therefore, these steps will be done according to the constraints which exist for the robot motion. Finally, the position of the knee joint and all joint angles are calculated using inverse kinematics.

## 2.1. Ankle Joint Trajectories

At this stage, the orientation of the foot, with respect to the ground and the position of ankle

$$x_a = \begin{cases} 0 & 0 \leq t \leq T_{dm2} \\ q_{fb} & t = T_d \\ q_{fm} & t = T_d + T_{sm} \\ q_{ff} & t = T_c \\ 0 & T_c + T_{dm1} \leq t \leq 2T_c \end{cases} \quad (1)$$

The position of the ankle joint in X direction ( $x_a$ ) must have these constraints in a

$$q_f = \begin{cases} 0 & 0 \leq t \leq T_{dm2} \\ L_{cf} (1 - \cos q_f) + L_{cm} \sin(q_f) & t = T_d \\ x_{am} & t = T_d + T_{sm} \\ 2D_c + L_{ab} (\cos(q_f) - 1) + L_{ab} \sin(q_f) & t = T_c \\ 2D_c & T_c + T_{dm1} \leq t \leq 2T_c \end{cases} \quad (2)$$

In Equation (2)  $x_{am}$  is considered to be  $D_c/2$ . The constraints assumed is consistent with heel-off and toe-off motions. If the heel-off motion is omitted, then  $q_{fb}=0$  and  $T_{dm2}=0$ . In the same way, if the toe-off motion is omitted, then  $q_{ff}=0$  and  $T_{dm1}=0$ . If the toe-off and

in X and Z directions, are calculated. The orientations of foot ( $q_f$ ) must have these constraints in a walking cycle:

walking cycle:

heel-off motions are omitted simultaneously, then both cases occur together.

Also, the constraints for the position of the ankle joint in Z direction ( $z_a$ ) are considered as follows:

$$z_a = \begin{cases} L_{cm} & 0 \leq t \leq T_{dm2} \\ L_{cf} \sin(q_f) + L_{cm} (1 - \cos q_f) & t = T_d \\ L_{cm} + z_{am} & t = T_d + T_{sm} \\ -L_{ab} \sin(q_f) + L_{cm} \cos(q_f) & t = T_c \\ L_{cm} & T_c + T_{dm1} \leq t \leq 2T_c \end{cases} \quad (3)$$

In Equation (3),  $z_{am}$  is a gait parameter and is considered to be equal to 0.1 meter.

Knowing these constraints and using appropriate spline curves, ankle joint trajectories could be determined.

## 2.2. Hip Joint Trajectories

To plan hip joint trajectories, position of hip in X and Z directions are needed same as before. For the sake of simplicity, the trunk is supposed to be vertical during motion.

For the position of hip joint in X direction ( $x_h$ ), the following constraints are assumed:

$$x_h = \begin{cases} x_{ed} & t = 0 \\ D_c - x_{sd} & t = T_d \\ D_c + x_{ed} & t = T_c \\ 2D_c - x_{sd} & t = T_c + T_d \\ 2D_c + x_{ed} & t = 2T_c \end{cases} \quad (4)$$

Also, for the position of hip in Z direction ( $z_h$ ), the following constraints are considered:

$$z_h = \begin{cases} Z_{h-min} & t = \frac{T_d}{2} \\ Z_{h-max} & t = T_d + \frac{T_s}{2} \\ Z_{h-min} & t = T_c + \frac{T_d}{2} \\ Z_{h-max} & t = T_c + T_d + \frac{T_s}{2} \end{cases} \quad (5)$$

### 2.3. Inverse Kinematics

The obtained positions of the ankle and hip joints are utilized to calculate knee joint position. According to Figure 3, the inverse kinematics leads to the following equations:

$$\begin{cases} (x_k - x_h)^2 + (z_k - z_h)^2 = L_{th}^2 \\ (x_k - x_a)^2 + (z_k - z_a)^2 = L_{sh}^2 \end{cases} \quad (6)$$

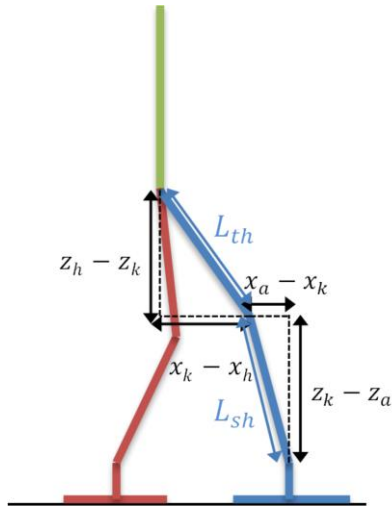


Fig. 3. Derivation of inverse kinematics formulation

These sets of equations have more than one answer, but the desired answer is determined according to the fact that the knee can only bend in one direction.

The joint angles are still unknown. The angle of each joint relative to the previous link can be calculated using the following relations:

$$\begin{cases} q_{tr} + q_h = \tan^{-1} \left( \frac{x_k - x_h}{z_k - z_h} \right) \\ q_{tr} + q_h + q_k = \tan^{-1} \left( \frac{x_a - x_h}{z_a - z_h} \right) \\ q_{tr} + q_h + q_k + q_a = q_f \end{cases} \quad (7)$$

$q_{tr}$  and  $q_f$  are the orientations of trunk and foot and  $q_h$ ,  $q_k$  and  $q_a$  are the hip, knee and ankle joint angles respectively.

Obtained position trajectories of all joints are shown in Figures 4 and 5. Also the joint angles calculated using inverse kinematics are shown in Figure 6.

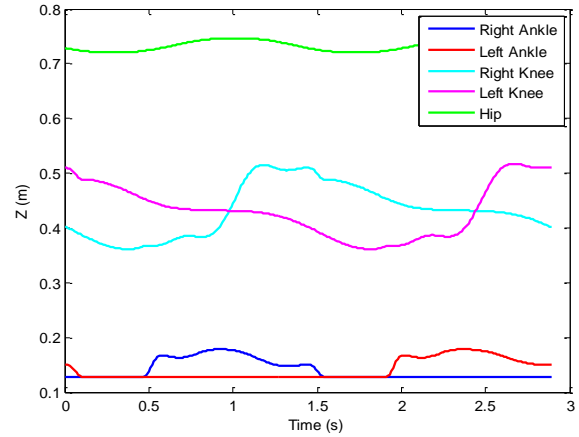


Fig. 4. The positions of joints in Z direction

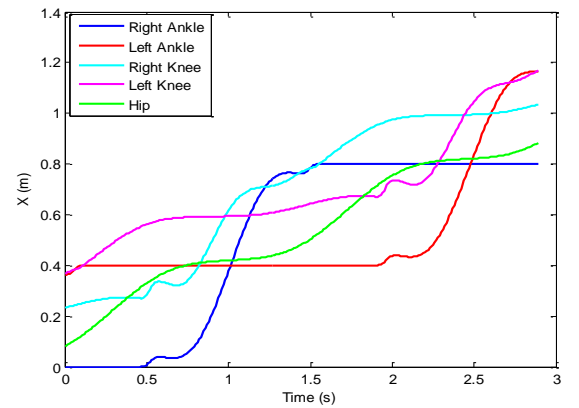


Fig. 5. The positions of joints in X direction

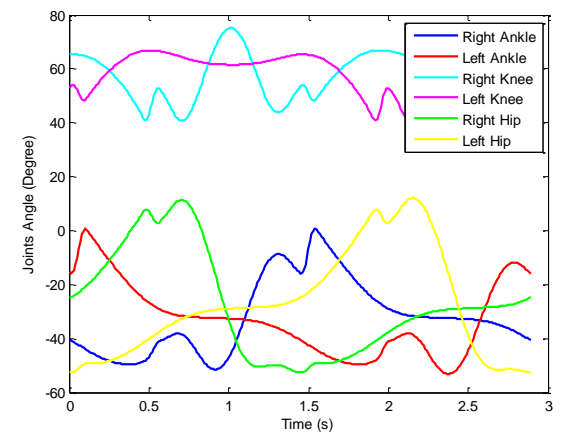


Fig. 6. The angle of joints

### 3. Dynamic Modelling

Here, the dynamic model of a 2D humanoid robot is obtained using two different methods: Lagrange and Kane. To this end, upper-body of the robot is assumed to be fixed, and the whole upper-body is modelled as a single rigid body.

#### 3.1. Dynamic model

The vector of generalized coordinate system describing the motion of the robot is defined as:

$$q = [q_{hR} \ q_{kR} \ q_{aR} \ q_{hl} \ q_{kl} \ q_{al} \ x_h \ z_h \ q_h]^T \quad (8)$$

The general form of the dynamic model of the robot is defined as follows:

$$M_{9 \times 9}(q) \times \ddot{q} + C_{9 \times 1}(q, \dot{q}) + G_{9 \times 1}(q) = Q \quad (9)$$

$M(q)$  shows the inertia matrix,  $C(q, \dot{q})$  denotes the Coriolis and centrifugal effects, and  $G(q)$  represents the effects of gravitational forces.

The dynamic model based on Lagrange method is calculated according to the following equations:

$$\frac{d}{dt} \left( \frac{\partial T}{\partial \dot{q}} \right) - \frac{\partial T}{\partial q} + \frac{\partial U}{\partial q} = Q$$

$$T = \sum_{i=0}^6 \frac{1}{2} m_i (\dot{x}^2 + \dot{z}^2) + \sum_{i=0}^6 \frac{1}{2} J_i \dot{q}_i^2 \quad (10)$$

$$U = \sum_{i=0}^6 m_i g z_i$$

and the Kane method is as follows:

$$\sum_{i=0}^6 (m_i [\ddot{x}_i \ \ddot{z}_i + g] \begin{bmatrix} \frac{\partial \dot{x}_i}{\partial \dot{q}} \\ \frac{\partial \dot{z}_i}{\partial \dot{q}} \end{bmatrix}) + \sum_{i=0}^6 (J_i \ddot{q}_i \frac{\partial \dot{q}_i}{\partial \dot{q}}) = Q \quad (11)$$

Equation (9) could be obtained by simplifying each of the Equations (10) or (11).

The right side of the Equation (9), which is the same as that of the Equations (10) and (11), changes with variations in the phase of the motion. The ground reaction forces, which are a part of the Q also change in different phases. These changes and the relation of Q and the ground forces are described in Table 4.

In Table 4,  $J$  is the Jacobian matrix of foot in the global coordinate system. Also  $\tau$ , which represents joint torques, is stated as:

$$\tau = [\tau_{hR} \ \tau_{kR} \ \tau_{aR} \ \tau_{hL} \ \tau_{kL} \ \tau_{aL}]^T \quad (12)$$

In order to complete the procedure, by substituting the term  $Q$  for each phase in Equation (9), the dynamic model of a 2D humanoid robot with heel-off and toe-off motion will be obtained, which is represented in the last column of Table 4.

To solve the dynamic model equations, firstly, the known and unknown parameters of the dynamic model equation should be specified. Based on the result of gait planning section, the left side of the Equation (9), which is a function of  $q$ ,  $\dot{q}$  and,  $\ddot{q}$ , was known.

The unknown parameters are joint torques and ground reactions, which represented as  $\begin{bmatrix} \tau \\ F \end{bmatrix}$  in

dynamic model equations. After substituting the known parameters in dynamic model Equations (9) and change the name of the unknown matrix to,  $X$  the general form of the dynamic model for each phase can be written as follows:

$$B = M(q) \ddot{q} + V(q, \dot{q}) + G(q) \quad (13)$$

$$AX = B$$

As represented in Table 4, the number of unknowns in DS phase is more than SS phase. Therefore, there are infinite numbers of answers for inverse dynamic problems in DS phase. All these infinite answers can be written in the following form:

$$X = A^\dagger B + (I - A^\dagger A)k \quad (14)$$

where  $A^\dagger$  represents Moore-Penrose pseudo-inverse of matrix  $A$ ,  $I$  is identity matrix, and  $k$  is an arbitrary constant vector.

Two answers, among these infinite answers are near to our goal:

- $X = A^\dagger B$ , in which norm of  $X$  is smaller than the norm of any other solution.
- $X$ , which is calculated based on Gaussian elimination. It has the fewest possible nonzero components.

The second answer yields to some zero ground reaction components which is not congruous with reality. Therefore, the first answer is chosen for solving inverse dynamic problem in DS.

Table 4. Walking pattern parameters

Motion Phase	Schema	Ground Reaction & Q	Dynamic Model
SS with Right Sole		$F_{sr} = [F_{x_r}, F_{z_r}, M_{y_r}]^T$ $Q = [B \quad J_{sr}^T]_{9 \times 9} \begin{bmatrix} \tau \\ F_{sr} \end{bmatrix}_{9 \times 1}$	$M_{9 \times 9}(q)\ddot{q} + V_{9 \times 1}(q, \dot{q}) + G_{9 \times 1}(q) = [B \quad J_{sr}^T]_{9 \times 9} \begin{bmatrix} \tau \\ F_{sr} \end{bmatrix}_{9 \times 1}$
DS with Both Soles		$F_{sr} = [F_{x_r}, F_{z_r}, M_{y_r}]^T$ $F_{sl} = [F_{x_l}, F_{z_l}, M_{y_l}]^T$ $Q = [B \quad J_{sr}^T \quad J_{sl}^T]_{9 \times 12} \begin{bmatrix} \tau \\ F_{sr} \\ F_{sl} \end{bmatrix}_{12 \times 1}$	$M_{9 \times 9}(q)\ddot{q} + V_{9 \times 1}(q, \dot{q}) + G_{9 \times 1}(q) = [B \quad J_{sr}^T \quad J_{sl}^T]_{9 \times 12} \begin{bmatrix} \tau \\ F_{sr} \\ F_{sl} \end{bmatrix}_{12 \times 1}$
DS with Right Sole and Left Heel		$F_{sr} = [F_{x_r}, F_{z_r}, M_{y_r}]^T$ $F_{hl} = [F_{x_l}, F_{z_l}, M_{x_l}, M_{z_l}]^T$ $Q = [B \quad J_{sr}^T \quad J_{hl}^T]_{9 \times 11} \begin{bmatrix} \tau \\ F_{sr} \\ F_{hl} \end{bmatrix}_{11 \times 1}$	$M_{9 \times 9}(q)\ddot{q} + V_{9 \times 1}(q, \dot{q}) + G_{9 \times 1}(q) = [B \quad J_{sr}^T \quad J_{hl}^T]_{9 \times 11} \begin{bmatrix} \tau \\ F_{sr} \\ F_{hl} \end{bmatrix}_{11 \times 1}$
DS with Right Toe and Left Sole		$F_{tr} = [F_{x_r}, F_{z_r}, M_{x_r}, M_{z_r}]^T$ $F_{sl} = [F_{x_l}, F_{z_l}, M_{y_l}]^T$ $Q = [B \quad J_{tr}^T \quad J_{sl}^T]_{9 \times 11} \begin{bmatrix} \tau \\ F_{tr} \\ F_{sl} \end{bmatrix}_{11 \times 1}$	$M_{9 \times 9}(q)\ddot{q} + V_{9 \times 1}(q, \dot{q}) + G_{9 \times 1}(q) = [B \quad J_{tr}^T \quad J_{sl}^T]_{9 \times 11} \begin{bmatrix} \tau \\ F_{tr} \\ F_{sl} \end{bmatrix}_{11 \times 1}$
DS with Right Toe and Left Heel		$F_{tr} = [F_{x_r}, F_{z_r}, M_{x_r}, M_{z_r}]^T$ $F_{sl} = [F_{x_l}, F_{z_l}, M_{y_l}]^T$ $Q = [B \quad J_{tr}^T \quad J_{sl}^T]_{9 \times 11} \begin{bmatrix} \tau \\ F_{tr} \\ F_{sl} \end{bmatrix}_{11 \times 1}$	$M_{9 \times 9}(q)\ddot{q} + V_{9 \times 1}(q, \dot{q}) + G_{9 \times 1}(q) = [B \quad J_{tr}^T \quad J_{sl}^T]_{9 \times 11} \begin{bmatrix} \tau \\ F_{tr} \\ F_{sl} \end{bmatrix}_{11 \times 1}$

Based on obtained equations of dynamic model, the unknown joint torques and ground reactions are calculated. In Figures 7 and 8, the calculated torques and ground reactions using the dynamic model are shown.

### 3.2. Verification of Dynamic Model

In order to verify the obtained dynamic model, two different methods are adopted: the first one computes the left side of the equation (9) with

$$X_{ZPM} = \frac{\sum_{i=1}^n x_{G_i} \times m_i (\ddot{z}_{G_i} + g) - \sum_{i=1}^n z_{G_i} \times m_i \ddot{x}_{G_i} - \sum_{i=1}^n \bar{I}_{y_i} \ddot{q}_{y_i}}{\sum_{i=1}^n m_i (\ddot{z}_{G_i} + g)} \quad (15)$$

both Kane and Lagrange methods and compares the results of these two methods. Both obtained results are the same; therefore, the obtained dynamic model is validated in one way.

The second method is based on the position of ZMP point calculated by two different approaches. The first approach is based on the kinematics of the robot as follows:

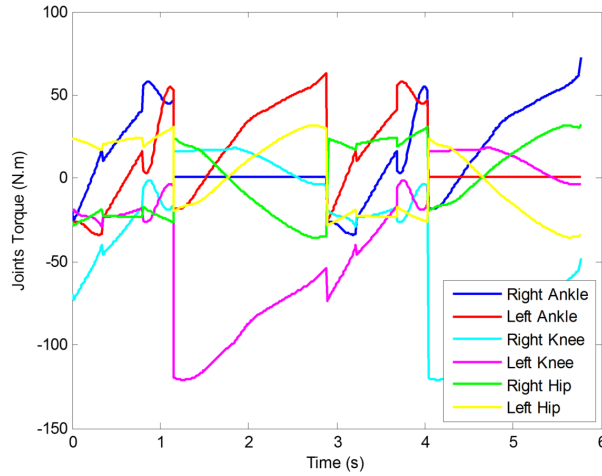


Fig. 7. Joint torques calculated by obtained dynamic model

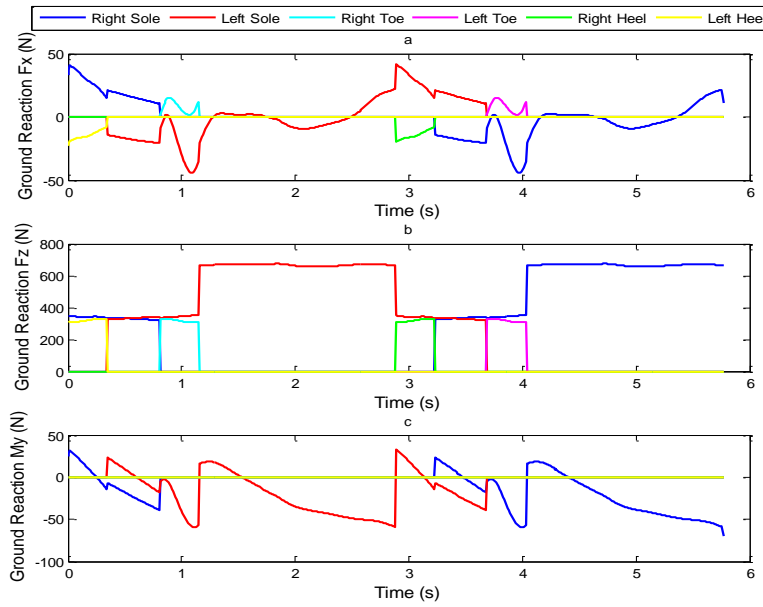


Fig. 8. a) Ground reaction  $F_x$ . b) Ground reaction  $F_z$ . c) Ground reaction  $M_y$

ZMP position may as well be obtained using ground reactions. In this case, the position of ZMP point in X direction is obtained using the following relation:

$$x_{zmp} = \frac{F_{zR}X_{soleR} + F_{zL}X_{soleL} - M_{yR} - M_{yL}}{F_{zR} + F_{zL}} \quad (16)$$

The ZMP position calculated using the kinematics of robot and ground reaction is similar as shown in Figure 9.

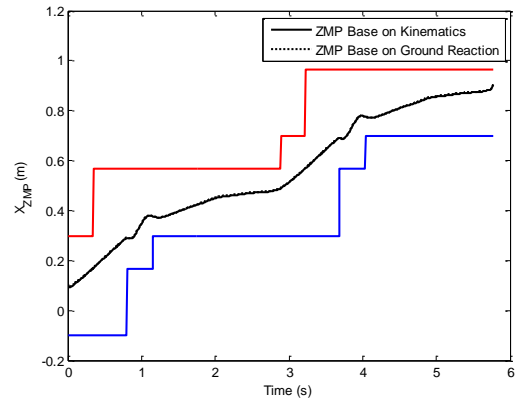


Fig. 9. The ZMP based on ground reaction and the ZMP based on kinematics

#### 4. Optimization

The main goal of this article is to obtain the optimized heel-off and toe-off angles. To this end, some optimization parameters should be determined first. Afterwards, objective functions should be defined which depend on the optimization parameters. Here, the objective is to optimize the energy consumption and the stability of the robot. At the end, the objective functions will be optimized using GA.

##### 4.1. Optimization Parameters

As mentioned, the first step is to determine the optimization parameters. The optimum value of these parameters will be determined during the optimization process. The candidate parameters for optimization are shown in Table 5. These parameters have already been introduced in Table 3.

Table 5. Optimization parameters

#	Optimization parameters
1	$D_c$
2	$X_{ed}$
3	$X_{sd}$
4	$Z_{h-min}$
5	$Z_{h-max}$
6	$q_{fb}$
7	$q_{ff}$
8	$q_{fm}$

##### 4.2. Objective Functions

Setting appropriate objective functions is one of the most challenging and important parts of the optimization process. Here, two main objective functions are introduced:

1. The first one calculates energy consumption per meter and is defined as follows:

$$J = \frac{-1}{D_c \int_0^{2r_c} (\dot{q}_a \tau_a + \dot{q}_k \tau_k + \dot{q}_h \tau_h) dt} \quad (17)$$

In Equation (17),  $\tau_h$ ,  $\tau_k$ , and  $\tau_a$  show hip, knee, and ankle joint torques and  $\dot{q}_h$ ,  $\dot{q}_k$ , and  $\dot{q}_a$  show the velocity of these joints respectively.

According to Equation (17), the value of  $J$  is always negative. As the energy consumption decreases, the value of  $J$  becomes smaller.

2. The second objective function defines the stability and could be defined as follows:

$$J = -1000 \times \min(x_{zmp} - SP) \quad (18)$$

In this function, minimum distances between the ZMP point and the support polygon [29] borders are calculated in millimeters. As the Equation (18) shows, if the motion is stable, then the ZMP point is inside the support polygon and the value of  $J$  becomes negative. Obviously, as the value of  $J$  becomes smaller, the stability increases.

These objective functions may lead to some undesired cases, including “singularity”, “foot impact” and “power limit”. To avoid these, some penalty functions are used. “Singularity” happens when the knee joint angle becomes zero. To avoid near singularity condition, knee joint must not become less than  $5^\circ$ . “Foot impact” occurs when the Z component of any point of foot becomes less than zero (ground level). Also, “power limit” means that the required power of joints exceed the maximum limit of actuators. These limitations translate into some functions called penalty functions. In this way, when each of these cases occurs, the penalty functions generate a large positive value as the goal function of GA algorithm.

#### 5. Results

After lots of trial and errors, the GA algorithm parameters are chosen as follows:

$$\begin{aligned} \text{Population Size} &= 100, \text{Crossover Fraction} = \\ &0.8, \text{Mutation Fraction} = 0.2 \end{aligned} \quad (19)$$

In Figure 10a, the optimized energy consumption for both optimizations are shown. The blue curve shows the optimized energy consumption for minimum energy consumption optimization and the red one shows the same results for the maximum stability optimization.

In Figure 10b, the optimized stability for both optimizations are shown. Same as Figure 10a, one of the curves shows the optimized stability for minimum energy consumption optimization, while the other shows the same results for maximum stability optimization.

In Figures 10c and 10d, the optimized heel-off and toe-off angles for both optimizations are illustrated, respectively.

Moreover, in Figure 11, the optimized values of the other optimization parameters are depicted.

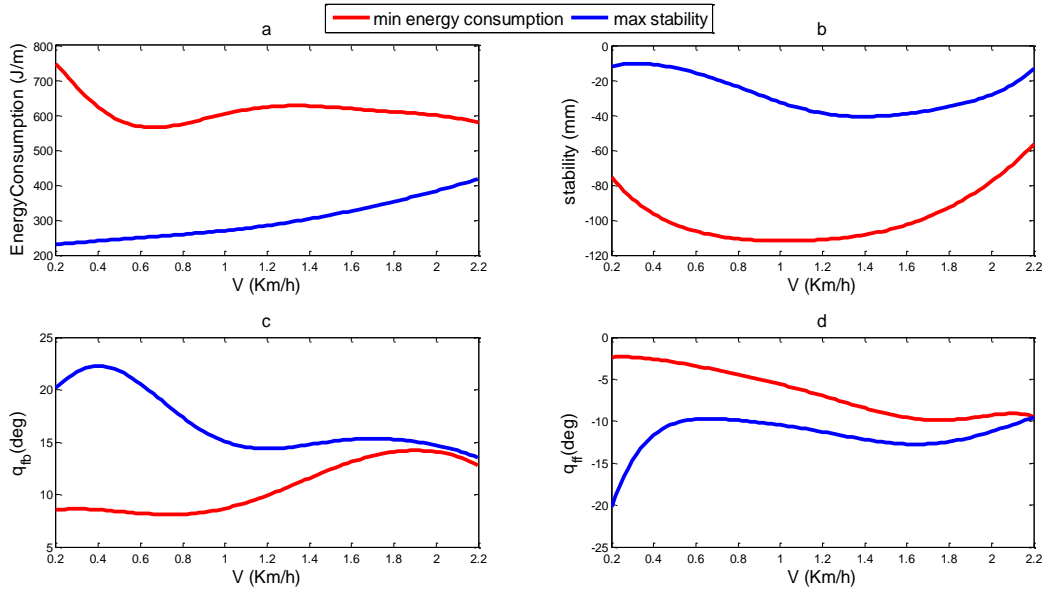


**Fig. 10.** a) The energy consumption of minimum energy consumption and maximum stability optimizations. b) The stability of minimum energy consumption and maximum stability optimizations. c) The toe-off angle with respect to velocity for two different optimizations. d) The heel-off angle with respect to velocity for two different optimizations.

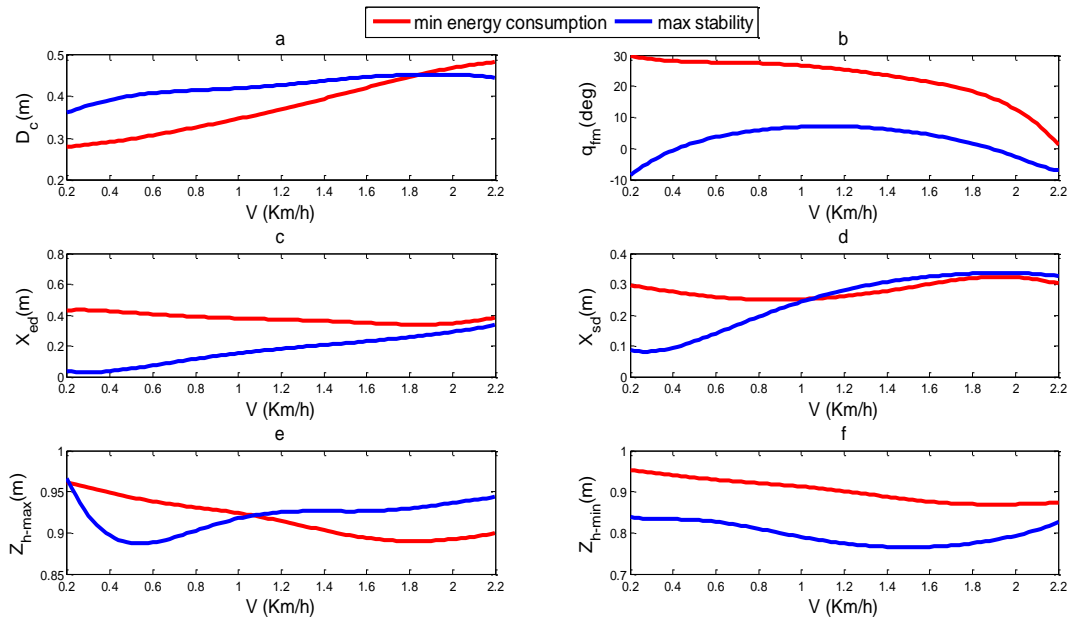


**Fig. 11.** a) The stride length with respect to velocity for two different optimizations. b) The  $q_{fm}$  with respect to velocity for two different optimizations. c) The  $X_{ed}$  with respect to velocity for two different optimizations. d) The  $X_{sd}$  with respect to velocity for two different optimizations. e) The  $Z_{h-max}$  with respect to velocity for two different optimizations. f) The  $Z_{h-min}$  with respect to velocity for two different optimizations.

In addition to optimization results, a parametric analysis has been done to inspect the effects of heel-off and toe-off motions on both objective functions more accurately. Therefore, two surfaces have been depicted for this inspection. Figures 12 and 13 show the results for the velocity of 1km/h. In Figures 12 and 13, the energy consumption and stability

margin for different heel-off and toe-off angles are shown, respectively. The optimum result for energy consumption objective function at this velocity is as follows:

$$\begin{aligned} \text{Min Energy Consumption} \Rightarrow \\ q_{ff} = 7^\circ, q_{fb} = 7^\circ \end{aligned} \quad (20)$$

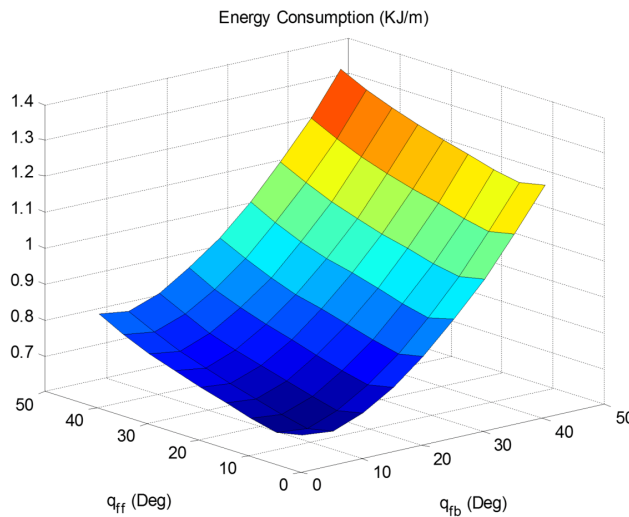


Fig. 12. Effects of  $q_{ff}$  and  $q_{fb}$  on the optimization of energy consumption

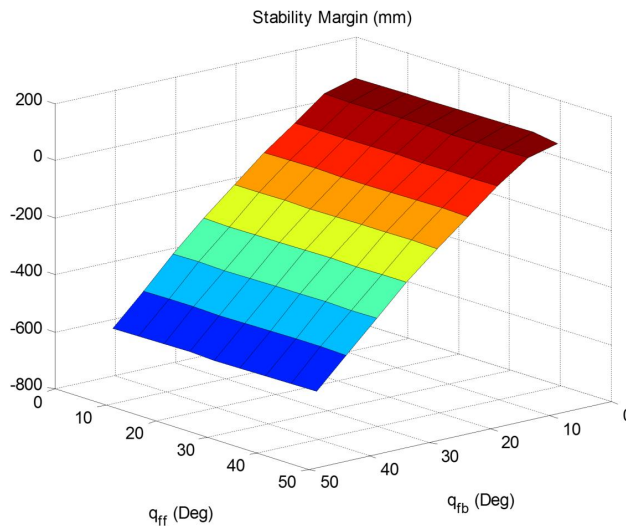


Fig. 13. Effects of  $q_{ff}$  and  $q_{fb}$  on the optimization of stability

### 6. Discussion

As it was shown in Figure 10a, the energy consumption for minimum energy consumption optimization is less than the energy consumption for maximum stability optimization in all velocities and there is a dramatic difference between these two curves.

In Figure 10b, the stability for maximum stability optimization is more than the stability for minimum energy consumption optimization in all velocities. Like the previous graph, there is a dramatic difference between the two curves. These two graphs show that the adopted objective functions minimize their objective functions truly.

In Figures 10c and 10d,  $q_{ff}$  and  $q_{fb}$  are represented with respect to velocity for two different optimizations, respectively. In both figures, the absolute value of  $q_{ff}$  and  $q_{fb}$  for the minimum energy consumption optimization is less than the maximum stability optimization. Therefore, for the maximum stability optimization, larger heel-off and toe-off angles are needed compared to the minimum energy consumption optimization. To interpret this behavior, it could be said that, the joints must prevent from dramatic changes of angle in order to consume less energy.

As represented in Figures 10c and 10d, as the velocity increases, the difference between two curves (minimum energy consumption and maximum stability) is decreased. That is because in high velocities there is a small number of feasible motions according to optimization limits. Therefore, the answers of both optimizations become similar and the two curves approach each other.

In Figure 11a-f, the results of other 6 optimization parameters, which have been introduced in Table 5, are depicted. As represented in Figure 11a, the step length increases with respect to the velocity for the minimum energy consumption optimization. However, the value of the step length does not have any considerable changes for the maximum stability optimization. Also, it could be observed that the optimum step length is small in low velocities for the minimum energy consumption optimization.

Some notable results are deduced from Figure 11f. As depicted in Figure 11f, the value of  $Z_{h-min}$  for minimum energy consumption optimization is always more than the value of this parameter for maximum stability optimization. On the other hand, large values for  $Z_{h-max}$  and  $Z_{h-min}$  lead to walking pattern with the knees stretched. Therefore, it could be concluded that, to consume less energy, the robot should walk with stretched knees.

As represented in Figures 12 and 13, there exists an optimum value for heel-off and toe-off angles which minimizes the energy consumption in each velocity. Another important conclusion results from Figure 13 which shows the trend of  $q_{ff}$  and  $q_{fb}$  for different stability margins. As depicted in Figure 13, the stability increases by increasing  $q_{fb}$  and

it approximately does not change by  $q_{ff}$ . The cause of this behavior returns to the fact that the robot tends to collapse backward, so the toe-off angle ( $q_{fb}$ ) plays an important role in the stability of robot. It should be noted that, if the heel-off angle increases more than human-like walking, then the walking pattern would not be natural and the energy consumption would increase abnormally. Hence, large toe-off angle is not desirable and should be avoided. As depicted in Figure 13, the robot will lose its stability if the heel-off angle becomes less than  $10^\circ$ .

In brief, to access stable motions in high velocities, less heel-off and toe-off motions are needed. Consequently, more heel-off and toe-off motions are needed for stable motions in low velocities. On the contrary, for minimum energy consumption optimization, large heel-off and toe-off angles lead to less energy consumption in high velocities and vice versa.

## 7. Conclusion

In this paper, the effects of heel-off and toe-off motions were studied on the motion of a 2D humanoid robot through the presented optimizations and parametric analysis. To this end, firstly a gait planning was done. Then, the dynamic model of the robot was derived using the Kane and Lagrange methods and it was verified by two different approaches. Finally, the optimization procedure using GA was done with two different objective functions which minimizes the energy consumption and maximizes the stability. According to the results, to have a more stable motion in low velocities, large heel-off and toe-off angles are needed. In high velocities, there exist a few numbers of feasible motions, therefore the results of both optimizations approach each other. On the other hand, to consume less energy in high velocities, large heel-off and toe-off angles are needed. The parametric analysis also inspected the effects of both heel-off and toe-off motions together on two different objective functions and found the optimum values for a specified velocity.

## References

1. P. Channon, S. Hopkins, and D. Pham, "Derivation of optimal walking motions for a

- bipedal walking robot," *Robotica*, vol. 10, pp. 165-172, 1992.
2. C. Chevallereau and Y. Aoustin, "Optimal reference trajectories for walking and running of a biped robot," *Robotica*, vol. 19, pp. 557-569, 2001.
  3. S. Kajita and K. Tani, "Study of dynamic biped locomotion on rugged terrain-derivation and application of the linear inverted pendulum mode," in *Robotics and Automation, in Proceedings of IEEE International Conference on*, 1991, pp. 1405-1411.
  4. S. Kajita, F. Kanehiro, K. Kaneko, K. Fujiwara, K. Harada, K. Yokoi, *et al.*, "Biped walking pattern generation by using preview control of zero-moment point," in *Robotics and Automation. Proceedings. ICRA'03. IEEE International Conference on*, 2003, pp. 1620-1626.
  5. J. H. Park and K. D. Kim, "Biped robot walking using gravity-compensated inverted pendulum mode and computed torque control," in *Robotics and Automation, In: Proceedings of the 1998 IEEE 1998*, pp. 3528-3533.
  6. T. Sato, S. Sakaino, and K. Ohnishi, "Real-time walking trajectory generation method with three-mass models at constant body height for three-dimensional biped robots," *Industrial Electronics, IEEE Transactions on*, vol. 58, pp. 376-383, 2011.
  7. Q. Huang, K. Yokoi, S. Kajita, K. Kaneko, H. Arai, N. Koyachi, *et al.*, "Planning walking patterns for a biped robot," *Robotics and Automation, IEEE Transactions on*, vol. 17, pp. 280-289, 2001.
  8. M. Rostami and G. Bessonnet, "Sagittal gait of a biped robot during the single support phase. Part 2: optimal motion," *Robotica*, vol. 19, pp. 241-253, 2001.
  9. G. Capi, Y. Nasu, L. Barolli, K. Mitobe, and K. Takeda, "Application of genetic algorithms for biped robot gait synthesis optimization during walking and going up-stairs," *Advanced robotics*, vol. 15, pp. 675-694, 2001.
  10. G. Bessonnet, S. Chesse, and P. Sardain, "Optimal gait synthesis of a seven-link planar biped," *The International journal of robotics research*, vol. 23, pp. 1059-1073, 2004.
  11. G. Bessonnet, P. Seguin, and P. Sardain, "A parametric optimization approach to walking pattern synthesis," *The International Journal of Robotics Research*, vol. 24, pp. 523-536, 2005.
  12. M. J. Sadigh and S. Mansouri, "Application of phase-plane method in generating minimum time solution for stable walking of biped robot with specified pattern of Motion," *Robotica*, vol. 31, pp. 837-851, 2013.
  13. G. Carbone, Y. Ogura, H.-o. Lim, A. Takamishi, and M. Ceccarelli, "Dynamic simulation and experiments for the design of a new 7-dofs biped walking leg module," *Robotica*, vol. 22, pp. 41-50, 2004.
  14. T. Buschmann, S. Lohmeier, and H. Ulbrich, "Humanoid robot lola: Design and walking control," *Journal of physiology-Paris*, vol. 103, pp. 141-148, 2009.
  15. D. Tlalolini, C. Chevallereau, and Y. Aoustin, "Comparison of different gaits with rotation of the feet for a planar biped," *Robotics and Autonomous Systems*, vol. 57, pp. 371-383, 2009.
  16. S. Aoi and K. Tsuchiya, "Generation of bipedal walking through interactions among the robot dynamics, the oscillator dynamics, and the environment: Stability characteristics of a five-link planar biped robot," *Autonomous Robots*, vol. 30, pp. 123-141, 2011.
  17. O. Kwon and J. H. Park, "Asymmetric trajectory generation and impedance control for running of biped robots," *Autonomous Robots*, vol. 26, pp. 47-78, 2009.
  18. S. Aoi and K. Tsuchiya, "Locomotion control of a biped robot using nonlinear oscillators," *Autonomous robots*, vol. 19, pp. 219-232, 2005.
  19. M. Sadedel, A. Yousefi-Koma, and M. Khadiv, "Offline path planning, dynamic modeling and gait optimization of a 2D humanoid robot," in *Robotics and Mechatronics (ICRoM), Second RSI/ISM International Conference on*, 2014, pp. 131-136.
  20. M. Khadiv, S. A. A. Moosavian, and M. Sadedel, "Dynamics modeling of fully-actuated humanoids with general robot-environment interaction," in *Robotics and Mechatronics (ICRoM), Second RSI/ISM International Conference on*, 2014, pp. 233-238.
  21. ] M. Khadiv, S. A. A. Moosavian, A. Yousefi-Koma, M. Sadedel, and S. Mansouri, "Optimal gait planning for humanoids with 3D structure walking on slippery surfaces," *Robotica*, pp. 1-19, 2015.
  22. T. Wang, C. Chevallereau, and C. F. Rengifo, "Walking and steering control for a 3D biped robot considering ground contact and stability," *Robotics and Autonomous Systems*, vol. 60, pp. 962-977, 2012.
  23. Y. Aoustin and A. Formalskii, "3D walking biped: optimal swing of the arms," *Multibody System Dynamics*, vol. 32, pp. 55-66, 2014.
  24. D. Tlalolini, C. Chevallereau, and Y. Aoustin, "Human-like walking: Optimal motion of a bipedal robot with toe-rotation motion," *Mechatronics, IEEE/ASME Transactions on*, vol. 16, pp. 310-320, 2011.

25. M. Vukobratovic and D. Juricic, "Contribution to the synthesis of biped gait," *Biomedical Engineering, IEEE Transactions on*, pp. 1-6, 1969.
26. A. Goswami, "Postural stability of biped robots and the foot-rotation indicator (FRI) point," *The International Journal of Robotics Research*, vol. 18, pp. 523-533, 1999.
27. M. B. Popovic, A. Goswami, and H. Herr, "Ground reference points in legged locomotion: Definitions, biological trajectories and control implications," *The International Journal of Robotics Research*, vol. 24, pp. 1013-1032, 2005.
28. H. Hirukawa, S. Hattori, S. Kajita, K. Harada, K. Kaneko, F. Kanehiro, et al., "A pattern generator of humanoid robots walking on a rough terrain," in *Robotics and Automation, IEEE International Conference on*, 2007, pp. 2181-2187.
29. M. Vukobratović and B. Borovac, "Zero-moment point-thirty five years of its life," *International Journal of Humanoid Robotics*, vol. 1, pp. 157-173, 2004.